Prediction of gas–liquid flow in an annular gap bubble column using a bi-dispersed Eulerian model

Gaël Raymond Guédon*, Giorgio Besagni, Fabio Inzoli

Politecnico di Milano, Department of Energy, via Lambruschini 4a, 20156 Milan, Italy

Abstract

We present and discuss numerical results from simulations of the air–water flow in an annular gap bubble column of 0.24 m internal diameter, at air superficial velocities ranging from 0.004 m/s to 0.225 m/s, covering the homogeneous and heterogeneous regimes. A bi-dispersed Eulerian model is implemented to account for both the stabilizing and destabilizing effects of small and large bubbles. Sensitivity studies on the mesh element size, time step size and number of outer iterations per time step are performed and optimal simulation parameters and mesh are used to predict the holdup curve. Comparison with two mono-dispersed models is provided to emphasize the necessity of a bi-dispersed approach for the accurate prediction of the homogeneous regime, given the poly-dispersed nature of the flow investigated. Two different approaches for the characterization of the small and large bubbles groups are also discussed. We found that the relative amount of small bubbles is an important input parameter for the present model and can be provided using available empirical correlations or experimental data. The results obtained from the simulations also demonstrated the necessity of a population balance model able to capture the bubbles coalescence and breakup phenomena for the correct prediction of the heterogeneous regime.

Keywords: Bubble column, CFD simulation, Bulk liquid turbulence, Holdup curve, Model validation, Poly-dispersed homogeneous regime

*Corresponding author. Tel.: +39 02 2399 3828.
Email address: gaelraymond.guedon@polimi.it (Gaël Raymond Guédon)

Highlights

- A bi-dispersed model is used to simulate an annular gap bubble column.

- Sufficiently fine mesh discretization is required to capture transient phenomena.

- Mono-dispersed models fail to predict experimental data in the homogeneous regime.

- Inclusion of large bubbles destabilizing effect is relevant for simulation accuracy.

- Total gas holdup is sensitive to small bubbles volume fraction input data.

1. Introduction

Bubble column reactors are well known for their low price-performance ratio wherever heat or mass transfer between various fluids is desired, such as in the chemical, petrochemical, food production or materials processing industries (Shah et al., 1982; Dudukovic, 1999). However, their main drawback is the difficult design and scale-up, due to the complex multiphase flow that builds up as flow rates and dimensions increase (Tarmy and Coulaloglou, 1992). Moreover, in most industrial applications, internal devices are often added to control heat transfer, to foster bubble break-up or to limit liquid phase back mixing (Youssef et al., 2013). These elements can have significant effects on the multiphase flow inside the bubble column reactor and the prediction of these effects is still hardly possible without experimentation (Youssef et al., 2013).

Annular gap bubble columns are reactors with vertical internal pipes. Understanding the two-phase flow inside such devices is relevant for some important practical applications. The influx of gas, oil and water inside a wellbore casing represents a multiphase flow inside concentric or eccentric annuli (Kelessidis and Dukler, 1989; Hasan and Kabir, 1992; Das et al., 1999a,b; Lage and Time, 2002).

2

Heat exchangers, water-cooled nuclear reactors, serpentine boilers and plunging jet reactors also constitute industrial equipments where a complex multiphase flow inside annuli occurs. The availability of experimental data on such configuration is however relatively scarce (Cumming et al., 2002; Al-Oufi et al., 2010; Al-Oufi et al., 2011; Besagni et al., 2014b,a, 2016; Besagni and Inzoli, 2016a,c). Predictive tools also still rely on empirical or semi-empirical models, which validity is limited to the operating conditions used in the calibration of the model coefficients.

In general, the global and local flow properties in bubble column reactors are related to the prevailing flow regime, which can be distinguished in the homogeneous and the heterogeneous regimes (Nedeltchev and Shaikh, 2013). The homogeneous regime – associated with small gas superficial velocities – is referred to as the regime where only "non-coalescence-induced" bubbles exist, e.g. as detected by the gas disengagement technique (Besagni and Inzoli, 2016b). The homogeneous regime can be further distinguished into the "pure homogeneous" (or "mono-dispersed homogeneous") regime and the "pseudo-homogeneous" (or "poly-dispersed homogeneous" or "gas maldistribution") regime. The transition from the homogeneous regime to the heterogeneous regime is a gradual process in which a transition flow regime occurs. The transition regime is identified by the appearance of the "coalescence-induced" bubbles (Besagni and Inzoli, 2016b) and is characterized by large flow macro-structures with large eddies and a widened bubble size distribution due to the onset of bubble coalescence. At high gas superficial velocities, a fully heterogeneous regime is reached; it is associated with high coalescence and breakage rates and a wide variety of bubble sizes. It is worth noting that, in a large diameter bubble column, the slug flow regime may not be detected because of the well-known Rayleigh–Taylor instabilities. The transitions between the different flow regimes depend on the operation mode, design parameters and working fluids of the bubble column. For example, using a sparger that produces mainly very small bubbles the homogeneous regime is stabilized (Mudde et al., 2009), whereas the mono-dispersed homogeneous regime may not exist if large bubbles are aerated (Besagni and

Inzoli, 2016a) up to a "pure heterogeneous regime" from the beginning (Ruzicka et al., 2001). Since in industrial-scale reactors the gas is usually aerated through large spargers with large orifices, a pseudo-homogeneous regime is expected at most.

Numerical modeling of bubble column reactors using computational fluid dynamics (CFD) is a promising way of predicting, without introducing much empirical factors, the complex multiphase flow developing inside bubble column reactors. The increasing interests in such a predictive tool is also due to the ongoing growth of efficient and economical computational resources during the last decade. Among the available modeling techniques, the Eulerian multi-fluid approach is the most pursed one to simulate bubble column reactors (Jakobsen et al., 2005). It treats each phase as inter-penetrating continua and relies on an ensemble averaging of the multiphase Navier–Stokes equations, which requires closures for the flow turbulence and inter-phase mass, momentum and energy exchanges. The accuracy of simulations based on such a modeling approach is strongly dependent on the closure models implemented and, at a lower level, on numerical aspects such as the mesh and time step sizes.

The pioneering works of Sokolichin and Eigenberger (1994), Becker et al. (1994), Grevskott et al. (1996) and Pan et al. (1999) have, for instance, demonstrated the capabilities of the Eulerian two-fluid modeling approach to correctly reproduce the flow features arising in rectangular bubble columns using two-dimensional simulations. For more accurate predictions of the turbulent quantities and bubble plume oscillation period, Pfleger et al. (1999), Sokolichin and Eigenberger (1999) and Mudde and Simonin (1999) demonstrated that three-dimensional simulations are required. Similar conclusions are drawn for cylindrical bubble columns by Ekambara et al. (2005).

Numerical diffusion arising from stable upwind schemes is another parameter to consider for the accuracy of bubble column reactor simulations. Oey et al. (2003) demonstrated that the first order upwind scheme for convection discretization generates a significant amount of numerical diffusion, that prevents the transient nature of the two-phase flow to emerge. They advice the

4

use of higher order schemes. The studies performed by Jakobsen et al. (1997), Sokolichin et al. (1997), Jakobsen (2002), Jakobsen et al. (2005) and Laborde-Boutet et al. (2009) also highlight the necessity of high order discretization schemes to correctly predict the flow instabilities, regardless of the closure models implemented.

Along with the accuracy of discretization schemes, mesh resolution is another parameter determining the size of the truncation error. A mesh independent solution is generally looked for and some mesh size sensitivity studies are available in the literature. Generally speaking, the variability of the results on the mesh size depends on the turbulence modeling approach implemented. Milelli (2002) and Lakehal et al. (2002) performed two- and three-dimensional large eddy simulations (LES) of dilute bubbly flows and noticed that the mesh size should be within both a higher and a lower bound in order to get a proper filter cut-off. On the other hand, simulations implementing Reynolds-averaged Navier–Stokes (RANS) turbulence models are less restrictive on the mesh size. Sokolichin and Eigenberger (1999) compared three-dimensional simulations of a rectangular bubble column using various mesh sizes and obtained mesh independent results for mesh sizes of about one centimeter. A similar conclusion was drawn by Laborde-Boutet et al. (2009) who studied churn-turbulent flow in a cylindrical bubble column. Díaz et al. (2008) obtained mesh independent results when their *medium* and *fine* meshes where implemented, however the results using their *coarse* mesh were closer to the experimental data. Krepper et al. (2007) studied mesh refinements in separate directions and did not found significant variations in final gas holdup, probably due to the already fine mesh sizes implemented. Frank et al. (2008) were able to get mesh independent results for medium mesh sizes when the Tomiyama's wall lubrication force was implemented rather than the Antal's one. More recently, Ziegenhein et al. (2015) studied meshes with various element sizes and aspect ratios and concluded that the results are more dependent on mesh element sizes in the transversal directions than in the vertical, or axial, direction. Though a number of mesh sensitivity studies were performed in the past, the proper mesh element

size to adopt in a bubble column reactor simulation is still an open debate (Ma et al., 2015a,b, 2016).

Aside from numerical aspects, proper turbulence modeling is important for the accuracy of simulations based on the Eulerian multi-fluid approach. In particular, it determines the rates of bubbles coalescence and break-up when a population balance model is implemented. Due to the complexity of turbulent phenomena, especially when multiple phases are involved, multiphase turbulence models are generally derived from their single-phase equivalent and terms modeling inter-phase interactions are added to the transport equations of the turbulence model (Pfleger et al., 1999). The multiphase equivalent of the standard $k - \epsilon$ model is the most widely adopted turbulence model in the studies reported in the literature (Borchers et al., 1999; Mudde and Simonin, 1999; Pfleger et al., 1999; Sokolichin and Eigenberger, 1999; Buwa and Ranade, 2002; Díaz et al., 2008; E. M. Cachaza et al., 2009; Guillen et al., 2011). Laborde-Boutet et al. (2009) recommend the use of the RNG $k - \epsilon$ model instead of the standard and realizable formulations due its greater performance on the case they studied, which involved a churn-turbulent flow in a circular bubble column. Zhang et al. (2006) compared simulations of bubbly flow using a $k - \epsilon$ model, supplemented by the bubble induced turbulence model of Pfleger and Becker (2001), with large eddy simulations and similar performances were obtained. Dhotre et al. (2008) also did a RANS-LES comparison and concluded that similar performances are obtained in terms of average quantities while more accurate liquid fluctuating velocities are achievable through LES, due to the limiting isotropic turbulence hypothesis of the $k - \epsilon$ model. Tabib et al. (2008) and Ekambara and Dhotre (2010) analyzed the performances of the $k - \epsilon$ and RSM turbulence models with LES and no significant differences were observed in terms of average quantities. Predicted fluctuating velocities are however more accurate when the RSM or LES turbulence modeling are used. The SST $k - \omega$ turbulence model has proven to be slightly superior to the $k - \epsilon$ model to simulate upward bubbly flow in the studies of Cheung et al. (2007a,b). It has also been used successfully in various recent research works to simulate two-phase flow in vertical pipes and

6

bubble columns (Frank et al., 2008; Duan et al., 2011; Rzehak and Krepper, 2013; Liao et al., 2014, 2015; Rzehak and Kriebitzsch, 2015; Rzehak et al., 2015; Ziegenhein et al., 2015; Besagni et al., 2016). The current focus is to study suitable turbulence modeling for the accurate estimate of the turbulent flow field, in order to give proper inputs to bubbles coalescence and break-up models. Among the RANS turbulence models, the ones able to predict turbulence anisotropy, such as the RSM family of models, are promising (Masood and Delgado, 2014; Masood et al., 2014; Pourtousi et al., 2014; Colombo and Fairweather, 2015).

In the Eulerian multi-fluid modeling approach, correlations for interfacial forces are implemented to model the inter-phase momentum exchanges. Interfacial forces are typically distinguished into the drag, lift, virtual mass, turbulent dispersion and wall lubrication forces, depending on the nature of the force which translates in a different mathematical formulation. The drag force determines the strongest inter-phase momentum exchange and influences the gas holdup and phases velocity (Tabib et al., 2008; Laborde-Boutet et al., 2009). The transversal lift force is responsible for the migration of small bubbles toward the column walls. On the other hand, a force that can be assimilated to the lift force tends to push large and deformed bubbles towards the center of the column (Tomiyama et al., 2002; Lucas et al., 2005). As a result, correlations for the lift coefficient usually display a change of sign from positive for small diameter bubbles to negative for large diameter bubbles. Lucas et al. (2005, 2006) also suggest that the lift force is responsible for the destabilization of homogeneous bubbly flow into heterogeneous flow. The virtual mass force arise from the relative acceleration of an immersed moving object to its surrounding fluid. As the object accelerates, it must accelerate the adjacent layers of the surrounding fluid, resulting in an interaction force acting on the object. Despite its apparent relevance in transient bubbly flows, this force is often found to be negligible in bubble columns simulations (Deen et al., 2001; Oey et al., 2003; Zhang et al., 2006; Díaz et al., 2008; Tabib et al., 2008; Masood and Delgado, 2014). Several studies also do not consider the inclusion of this force for this reason (Chen et al., 2004, 2005a,b; Larachi et al., 2006; Cheung et al., 2007a,b; Lucas et al.,

2007; Frank et al., 2008; Krepper et al., 2008; Díaz et al., 2009; Laborde-Boutet et al., 2009; Besagni et al., 2014a; Liao et al., 2014; Masood et al., 2014, 2015; Pourtousi et al., 2015b,a,c; Besagni et al., 2016). On the other hand, the recent work of Ziegenhein et al. (2015) demonstrated that the virtual mass force has an influence on the prediction of the turbulence intensity at higher flow rates. The bubbles dispersion due to the liquid turbulent fluctuations is taken into account through the turbulent dispersion force. It has an important role on the gas fraction profiles as it modulates peaks of small bubbles near the pipe walls and spreads out large bubbles from the pipe center (Lucas et al., 2007). Its magnitude is also high near distributor inlets (Krepper et al., 2007), supporting the modeling of bubbles dispersion near coarse spargers. Finally, the wall lubrication force is intended to model the lift force appearing close to the wall, that pushes the bubbles away from it. Rzehak et al. (2012) compared various formulations applied to vertical bubbly flow in a pipe and concluded that the inclusion of this force into the model is fundamental. They found that the correlation by Hosokawa et al. (2002) gives the best performances on the case studied.

Most of these correlations require as an input the average equivalent diameter of the bubbles, which determines the magnitude of the exchanges and eventually the direction of the interfacial forces, such as for the lift force (Tomiyama et al., 2002). The most common approach is to provide the bubbles equivalent diameter as a constant into the model, which value is mainly given by experimental data or correlations. Another approach is to implement a population balance model that predicts the local bubble size distributions from the fluid flow conditions using coalescence and breakage kernels (Lehr and Mewes, 2001; Buwa and Ranade, 2002). In this case, the gas phase is subdivided into several bubble size classes. The population balance equation of each class is then solved using the gas and liquid phase velocity fields information and the bubble size distribution at the inlet, that is given as a boundary condition. A single or multiple gas velocity fields can be implemented depending on the desired level of distinction between small and large bubbles. Multiple gas velocity fields or velocity groups

8

also lead to higher computational costs. Population balance models implement-
ing a single gas velocity field is referred to as homogeneous (Lo, 1996), while it
is referred to as inhomogeneous (Krepper et al., 2008) when multiple velocity
groups are solved. Homogeneous population balance models have been applied
to bubble column simulations and upward bubbly flows by several authors (Lehr
and Mewes, 2001; Buwa and Ranade, 2002; Chen et al., 2004, 2005a,b; Cheung
et al., 2007a,b; Díaz et al., 2008, 2009; Xu et al., 2013). On the other hand,
Krishna et al. (2000) introduced one of the first use of two velocity groups to
distinguish the dynamics of small and large bubbles. The model however did
not implement a population balance model but a constant bubble equivalent di-
ameter for each group. Further results using this approach were also presented
in van Baten and Krishna (2001), Krishna and van Baten (2001), van Baten
and Krishna (2002) and Xu et al. (2013). It is worth noting, though, that these
simulations only included the drag force. Recently, simulations implementing
two velocity groups for the gas phase and also including non-drag forces have
been presented by Ziegenhein et al. (2015) and Besagni et al. (2016). In these
studies, the bubble equivalent diameter of the two groups are computed from
the experimental bubble size distributions measured in the developed region,
for the various gas flow rates analyzed. More specifically, these distributions are
split up at the diameter for which the lift coefficient changes its sign, and the av-
erage diameters of the small and large bubbles groups are computed from their
corresponding distribution. In this way, the different dynamics of small and
larges bubbles resulting from a different lift force is included into the model.
This subdivision approach has been firstly introduced in simulations using a
population balance model by Krepper et al. (2005). It has been then applied
successfully in several studies (Lucas et al., 2007; Frank et al., 2008; Krepper
et al., 2008; Duan et al., 2011; Guillen et al., 2011; Lucas and Tomiyama, 2011;
Liao et al., 2014, 2015; Rzehak et al., 2015). In Xu et al. (2013), a comparative
study of the above mentioned approaches is proposed and the best performances
are given by the inhomogeneous population balance model.

The present work is about the application of a bi-dispersed Eulerian model

9

to simulate the air–water flow in an annular gap bubble column reactor of 0.24 m internal diameter, at gas superficial velocities ranging from 0.004 m/s to 0.225 m/s. The gas phase is subdivided into two classes, identified as *small* and *large* bubbles groups, and a velocity field for each class is solved. A constant bubble equivalent diameter is provided for each group based on two approaches: *(a)* an arbitrary method that follows considerations on the lift coefficient, and *(b)* a method that uses experimental bubble size distributions. The volume fraction of small and large bubbles at the inlet is set approximately according to *(a)* empirical correlations by Lemoine et al. (2008), and *(b)* image analysis data from experiments. The turbulence intensity at the inlet is given according to a correlation for bulk turbulence intensity in bubble columns (Kawase and Moo-Young, 1989). The turbulence model, the set of interfacial forces and the experimental data used for comparison are taken from previous studies (Besagni et al., 2016; Besagni and Inzoli, 2016a,c). In order to determine the proper mesh element size, a sensitivity study is performed. Then the optimized model is applied for the range of gas superficial velocities investigated. Diverse simulations using a mono-dispersed Eulerian model are also performed for comparison.

The paper is organized as follows. In Section 2 the experimental setup is presented, in Section 3 the governing equations, interfacial forces and boundary conditions are described, in Section 4 the sensitivity study on the mesh element size is presented, in Section 5 the results are presented and compared with experimental data, and finally conclusions are drawn in Section 6.

2. Experimental setup and dataset

The experimental facility (Figure 1) consists of a non-pressurized vertical column made of Plexiglas with an inner diameter $d_c = 0.24$ m and a height $H_c = 5.3$ m. Two internal pipes made of polyvinyl chloride are placed inside the column: one centrally positioned (with an external diameter of 0.06 m) and one asymmetrically positioned (with an external diameter of 0.075 m). A pressure regulator controls the air pressure upstream the two rotameters used
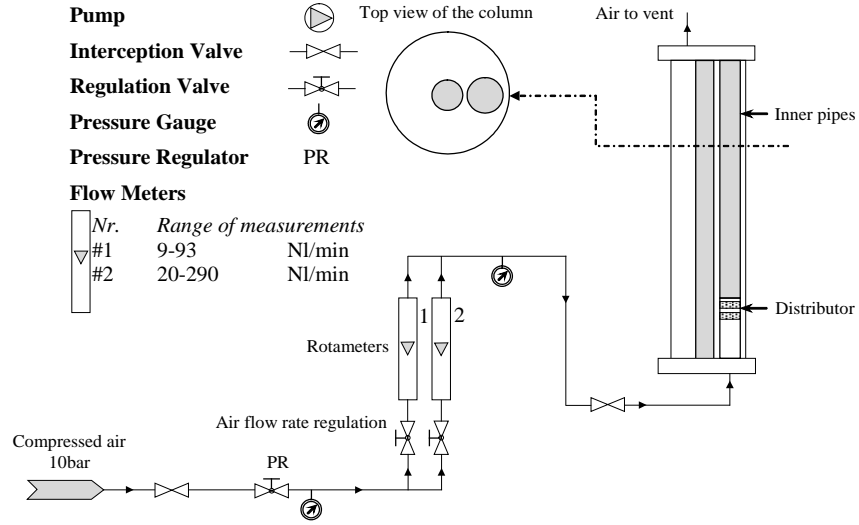
10

Figure 1: Experimental facility.

to measure the air flow rate. The air distributor is a tube made of stainless steel with an external diameter of 0.07 m and a height of 0.34 m. It is positioned asymmetrically on the lateral pipe and it is perforated along the circumference with holes of diameter $d_{\text{holes}} = 3.5$ mm at two vertical positions: a first row of holes at 0.2 m from the bottom of the column and a second row of holes at 0.3 m from the bottom of the column. Clean filtered deionized water was used and the initial water free surface location (height) is $H_0 = 3.245$ m (aspect ratio $H_0/d_c = 13.5$). During the experiments, the air and water temperatures were controlled to maintain constant values.

In this study, the gas holdup data obtained by measuring the bed expansion are used for the comparison with the numerical results. More details on the experimental procedure and measurement techniques are available in Besagni et al. (2016); Besagni and Inzoli (2016a,c).

Two main transitions exist in large diameter bubble columns (the reader should refer to the introduction for the discussion about flow regimes and the definition of the homogeneous regime):

11

₂₈₉ • the transition between the homogeneous and the transition regimes;

₂₉₀ • the transition between the transition and the heterogeneous regimes.

₂₉₁ However, in the literature, many authors consider only the first regime transi-
₂₉₂ tion, without any reference to the second one, except for a limited number of
₂₉₃ studies. In the following, for the sake of clarity, we refer to the "flow regime
₂₉₄ transition point" by considering the first transition point. Although the tran-
₂₉₅ sition from the homogeneous to the heterogeneous regime does not occur in-
₂₉₆ stantaneously, the definition of an approximate transition point is helpful to
₂₉₇ understand and model the hydrodynamic behavior of bubble columns (Krishna
₂₉₈ et al., 1991). The transition gas superficial velocity used to distinguish the ho-
₂₉₉ mogeneous regime from the heterogeneous one is determined using a combined
₃₀₀ analysis based on the Wallis plot of the data and the swarm velocity trend, as
₃₀₁ described in Besagni and Inzoli (2016c).

₃₀₂ The values of gas density (used to compute the gas superficial velocity) are
₃₀₃ based upon the operating conditions existing at the column midpoint (Reilly
₃₀₄ et al., 1994). The midpoint column pressure was assumed equal to the column
₃₀₅ outlet pressure plus one-half the total experimental hydrostatic pressure head.

₃₀₆ 3. Numerical model

₃₀₇ The numerical model is based on an Eulerian multi-fluid formulation and
₃₀₈ has been implemented in the commercial software ANSYS Fluent release 15.0.7.
₃₀₉ Each part of the model will be described in the following subsections.

₃₁₀ 3.1. Geometry and mesh

₃₁₁ A geometrical representation of the real experimental facility is used to per-
₃₁₂ form the simulations. The boundary of the domain is determined by the cylin-
₃₁₃ drical column of inner diameter 0.24 m and the two internal pipes of 0.06 m
₃₁₄ and 0.075 m outer diameters. The height of the domain is limited to 5 m.
₃₁₅ The sparger is modeled as a uniform cylindrical surface with a height of 0.01

12

Table 1: Characteristics of the meshes implemented.

Mesh	Horizontal mesh size Δ_h [m]	Vertical mesh size Δ_v [m]	Number of cells [-]
coarse	0.0150	0.0150	60 700
medium	0.0100	0.0100	196 000
fine	0.0067	0.0067	816 000
optimized	0.0067	$0.0134 \div 0.0268$	340 000

m placed on the lateral inner pipe at the vertical position of 0.3 m from the bottom of the domain. For the position of the inner pipes, refer to Figure 1.

The fluid domain is discretized using hexahedra and various mesh element sizes are analyzed. The relative performances of four meshes, namely *coarse*, *medium*, *fine* and *optimized*, are compared in Section 4. The characteristics of these meshes are summarized in Table 1. For the first three meshes, the element dimensions are uniform in all the directions, while for the *optimized* mesh, the element size is larger in the vertical direction so that an aspect ratio of 2 is present in the bulk flow region, i.e., up to about 3.5 m, and an aspect ratio of 4 is present above the free-surface, with a gradual transition between the two zones.

3.2. Governing equations

Within the Eulerian multi-fluid framework, two or more sets of Navier-Stokes equations are ensemble-averaged, and the effects of turbulence and inter-phase phenomena are taken into account using closure models. For an isothermal flow without mass transfer, the U-RANS governing equations for the k-th phase are

$$\frac{\partial}{\partial t}\left(\alpha_k \rho_k\right) + \nabla \cdot \left(\alpha_k \rho_k \mathbf{u}_k\right) = 0 \tag{1}$$

$$\frac{\partial}{\partial t}\left(\alpha_k \rho_k \mathbf{u}_k\right) + \nabla \cdot \left(\alpha_k \rho_k \mathbf{u}_k \mathbf{u}_k\right) = -\alpha_k \nabla p + \nabla \cdot \left(\alpha_k \bar{\tau_k}\right) + \alpha_k \rho_k \mathbf{g} + \mathbf{M}_{I,k} \tag{2}$$

The second term on the right-hand side of Eq. 2 includes the viscous and Reynolds stresses, while the third and last terms are respectively the gravity and the interfacial momentum exchanges between the phases. The latter

13

comprises diverse independent physical mechanisms: drag, lift, virtual mass, turbulent dispersion, and wall lubrication forces

$$\mathbf{M}_{I,k} = \mathbf{F}_{D,k} + \mathbf{F}_{L,k} + \mathbf{F}_{\mathrm{VM},k} + \mathbf{F}_{\mathrm{TD},k} + \mathbf{F}_{\mathrm{WL},k} \tag{3}$$

The present study includes two classes, or groups, of bubbles to account for the dynamics of small and large bubbles. As such, the water is considered the continuous phase and air is modeled using two dispersed phases with a distinct equivalent bubble diameter.

3.3. Interfacial momentum exchanges

The proper set of closure models for interfacial momentum exchanges to implement in a multi-fluid model is still an open debate. The actions of all the forces on the fluid dynamics being intrinsically coupled, individual validation of each single force is not possible. Instead, an entire set of interfacial forces should be implemented and compared with reference data. A thorough discussion on this aspect can be found in Rzehak and Krepper (2013).

Our numerical model implements the drag, lift, turbulent dispersion, and wall lubrication forces for both the bubbles classes. The expression for these forces will be given for a dispersed phase j in a continuous phase k (water, in this study). The source term for the continuous phase is then equal to the negation of the sum of the dispersed phase source terms

$$\mathbf{F}_k = -\sum_{j=1}^{2} \mathbf{F}_j \tag{4}$$

3.3.1. Drag force

The drag force is a resistive force arising from the presence of a relative motion of two phases. Its implementation within the ANSYS Fluent software reads

$$\mathbf{F}_{D,j} = -\frac{3}{4}\alpha_j \left(1 - \alpha_j\right)\rho_k \frac{C_D}{d_{b,j}}\left|\mathbf{u}_j - \mathbf{u}_k\right|\left(\mathbf{u}_j - \mathbf{u}_k\right) \tag{5}$$

where C_D is the drag coefficient. In the present study, the drag coefficient between the continuous phase (water) and the dispersed phases (air) is calculated

14

according to the correlation of Tomiyama et al. (1998) for bubbly flow in slightly contaminated water

$$\mathbf{C}_D = \max\left[\min\left(\frac{24}{\mathrm{Re}_b}\left(1 + 0.15\mathrm{Re}_b^{0.687}\right), \frac{72}{\mathrm{Re}_b}\right), \frac{8}{3}\frac{\mathrm{Eo}}{\mathrm{Eo} + 4}\right] \tag{6}$$

In this formulation, C_D depends on the bubble Reynolds number

$$\mathrm{Re}_b = \frac{\rho_k \left|\mathbf{u}_j - \mathbf{u}_k\right| d_{b,j}}{\mu_k} \tag{7}$$

and the Eötvös number

$$\mathrm{Eo} = \frac{g \left|\rho_k - \rho_j\right| d_{b,j}^2}{\sigma_{jk}} \tag{8}$$

No drag force interaction is taken into account between the two dispersed phases.

3.3.2. Lift force

The lift force is a transverse force originating in a shear flow. It is implemented as

$$\mathbf{F}_{L,j} = -C_L \alpha_j \rho_k \left(\mathbf{u}_j - \mathbf{u}_k\right) \times \left(\nabla \times \mathbf{u}_k\right) \tag{9}$$

The lift coefficient C_L depends mainly on the shape and dimension of the bubble. For small spherical bubbles, C_L is positive while it is negative for large deformed bubbles. The change of sign is due to an additional transverse force arising as bubbles become larger and deformed (Tomiyama et al., 2002; Lucas et al., 2005). To represent the different dynamics of small and large bubbles, the lift coefficient correlation of Tomiyama et al. (2002) is implemented together with the use of two bubble classes. For the air–water system at ambient conditions, the bubble diameter at which the change in sign occurs is 5.8 mm. The lift coefficient according to Tomiyama et al. (2002) is given as

$$C_L = \begin{cases} \min\left[0.288\tanh\left(0.121\mathrm{Re}_b\right), f\left(\mathrm{Eo}_\perp\right)\right] & \mathrm{Eo}_\perp \leq 4 \\ f\left(\mathrm{Eo}_\perp\right) & 4 < \mathrm{Eo}_\perp \leq 10 \\ -0.27 & 10 < \mathrm{Eo}_\perp \end{cases} \tag{10}$$

with

$$f\left(\mathrm{Eo}_\perp\right) = 0.00105\mathrm{Eo}_\perp^3 - 0.0159\mathrm{Eo}_\perp^2 - 0.0204\mathrm{Eo}_\perp + 0.474 \tag{11}$$

15

where $\mathrm{Eo}_\perp$ is the Eötvös number considering the maximum horizontal dimension of the bubble, $d_\perp$, given by the empirical correlation for the aspect ratio by Wellek et al. (1966)

$$d_\perp = d_{b,j} \left(1 + 0.163\mathrm{Eo}^{0.757}\right)^{1/3} \tag{12}$$

3.3.3. Turbulent dispersion force

The turbulent dispersion force has the purpose to model the diffusion effect of the turbulent fluctuations of the liquid phase on the bubbles. The mathematical expression of the force is derived by Favre averaging the inter-phase drag term and diverse formulations are available depending on the procedure followed during the derivation. The model of Burns et al. (2004) is implemented and reads as

$$\mathbf{F}_{\mathrm{TD},j} = -\frac{3}{4}C_{\mathrm{TD}}\alpha_j\left(1 - \alpha_j\right)\frac{C_D}{d_{b,j}}\left|\mathbf{u}_j - \mathbf{u}_k\right|\frac{\mu_k^{\mathrm{turb}}}{\sigma_{jk}}\left(\frac{\nabla\alpha_j}{\alpha_j} - \frac{\nabla\alpha_k}{\alpha_k}\right) \tag{13}$$

where $C_{\mathrm{TD}} = 1$, $\sigma_{jk} = 0.9$, and μ_k^{turb} is the turbulent viscosity of the continuous phase k.

3.3.4. Wall lubrication force

A bubble moving near a wall is subject to a lift force that pushes it away from the wall. This force is often mentioned as the wall lubrication force and is implemented as

$$\mathbf{F}_{\mathrm{WL},j} = -C_{\mathrm{WL}}\rho_k\alpha_j\left|\left(\mathbf{u}_k - \mathbf{u}_j\right)_\parallel\right|^2\mathbf{n}_w \tag{14}$$

where $\left(\mathbf{u}_k - \mathbf{u}_j\right)_\parallel$ is the relative velocity component parallel to the wall and $\mathbf{n}_w$ is the unit normal to the wall pointing toward the fluid. C_{WL} is the wall lubrication coefficient, which depends mainly on the distance to the wall and is given here by the model of Antal et al. (1991)

$$C_{\mathrm{WL}} = \max\left(0, \frac{C_{W1}}{d_{b,j}} + \frac{C_{W2}}{y_w}\right) \tag{15}$$

where $C_{W1} = -0.01$ and $C_{W2} = 0.05$ are dimensionless constants and y_w is the distance to the nearest wall.

16

3.4. Turbulence modeling

The effect of turbulence are included in the simulations through the use of an eddy diffusivity approach. The two equation $k - \omega$ shear-stress-transport (SST) turbulence model is implemented to estimate the Reynolds stresses, as suggested in Ziegenhein et al. (2015); Rzehak and Krepper (2013). The constants of the model follow their single phase counterparts. In the present implementation, turbulence effects in the liquid phase induced by the bubbles have been neglected. This is a matter of future studies.

3.5. Bubble size

Two dispersed phases representing *small* and *large* bubbles groups (or classes) are implemented in the model. Respectively, the first group includes bubbles for which the lift coefficient C_L is positive ($d_b < 5.8$ mm for the air–water system), while the second group includes bubbles for which the lift coefficient C_L is negative ($d_b > 5.8$ mm for the air–water system). Diverse approaches can be followed to determine the average equivalent diameter of each group, e.g. using: *(a)* empirical correlations, *(b)* a population balance model, *(c)* experimental measurements, or *(d)* considerations on the lift coefficient. The empirical correlations proposed by Lemoine et al. (2008) could be used, however it over-predicts small bubbles diameters when compared to our experimental data (Besagni and Inzoli, 2016a). This is probably due to their different definition of small and large bubbles groups. Implementing a population balance model may be the most suitable method however it has additional computational costs and is matter of future studies. When experimental bubble size distributions (BSD) are available, the average equivalent diameter of each group can be calculated splitting the BSD at the diameter at which the lift coefficient changes its sign, as illustrated in Figure 2, and computing the Sauter mean diameter of each sub-BSD as follow

$$d_b = \frac{\displaystyle\sum_{i=1}^{N} n_i d_{b,i}^3}{\displaystyle\sum_{i=1}^{N} n_i d_{b,i}^2} \tag{16}$$

17
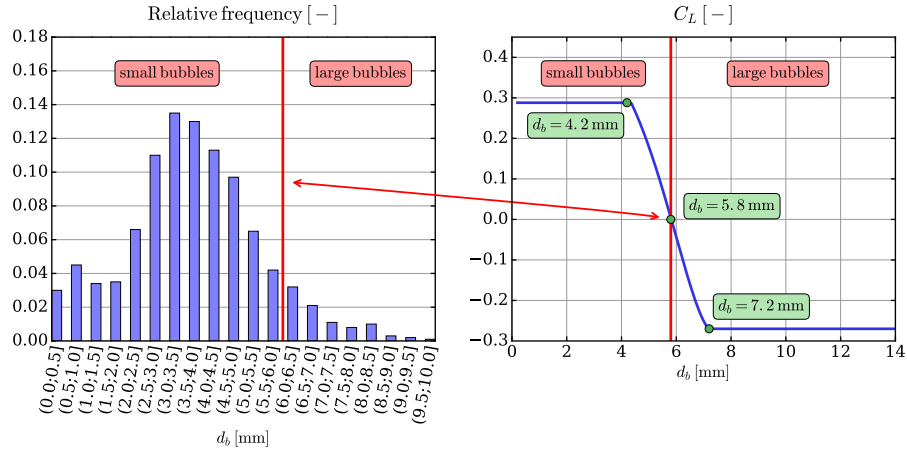
Figure 2: Bi-dispersed approach: splitting the BSD into two groups of bubbles. The lift coefficient is given for $\text{Re}_b > 30$.

where $d_{b,i}$ and n_i are the diameter and the number of bubbles of size class i, respectively, and N is the number of size classes in the sub-BSD. Finally, when reference data are not available, arbitrary equivalent diameters can be implemented and we suggest that their values should be set according to the lift coefficient value, e.g. at $\text{Eo}_\perp \approx 4$ for the small bubbles group and at $\text{Eo}_\perp \approx 10$ for the large bubbles group (see illustration in Figure 2). In this way, most of the dynamics of each bubbles group is captured and discrepancies may be mainly due to slightly over- or under-estimated drag forces.

In this study, the latter method will be used for all the gas superficial velocities investigated. Moreover, experimental bubble size distributions (BSD) obtained from digital image analysis of the developed flow region are available for three gas superficial velocities $U_G = 0.0087, 0.0220$, and 0.0313 m/s (Besagni and Inzoli, 2016a). As a consequence, additional results using the experimental equivalent diameters at these gas superficial velocities will be shown for comparison. The diameters implemented in the simulations are listed in Table 2 according to the method used.

18

Table 2: Implemented equivalent bubble diameters, d_b, according to the input method used.

Input method	Group	U_G [m/s]			
		0.0087	0.0220	0.0313	others
Arbitrary	*small*	4.2 mm	4.2 mm	4.2 mm	4.2 mm
	large	7.2 mm	7.2 mm	7.2 mm	7.2 mm
Experimental	*small*	4.18 mm	4.31 mm	4.29 mm	-
BSD	*large*	7.38 mm	7.27 mm	7.31 mm	-

Table 3: Air and water density and dynamic viscosity, and surface tension coefficient of the air–water system at the averaged operating conditions.

Phase	Density	Dynamic viscosity	Surface tension coefficient
	[kg/m^3]	[kg/ms]	[N/m]
Air	1.359	1.85×10^{-5}	-
Water	997	8.9×10^{-4}	-
Air–Water	-	-	0.072

3.6. Fluid properties

Both fluid phases are considered incompressible despite the air phase experiences a slight variation of density from the bottom to the top of the column due to the hydrostatic pressure. The fluid properties are taken at the averaged conditions $p = 1.16$ bar and $T = 25$ °C and are listed in Table 3

3.7. Initial and boundary conditions

The column is initially filled with water up to 3 m above the sparger, as in the experiments, and null velocities are set. Velocity inlet boundary conditions are assigned at the sparger for the two groups of air bubbles, and outflow conditions are assigned at the outlet for each phase. The volume fraction and the equivalent diameter of *small* and *large* bubbles at the inlet are set according to *(a)* correlations for small and large bubbles volume fractions by Behkish et al. (2006) for the arbitrary method, and *(b)* volume fractions from experimental

Table 4: Gas volume fractions, α_G, of the *small* and *large* bubbles at the inlet.

Input method	Group	U_G [m/s]			
		0.0087	0.0220	0.0313	other
Arbitrary	*small*	0.485	0.526	0.540	Behkish et al. (2006)
	large	0.515	0.474	0.460	Behkish et al. (2006)
Experimental	*small*	0.53	0.45	0.42	-
BSD	*large*	0.47	0.55	0.58	-

digital image analyses for the experimental BSD method. Table 4 lists the values given by the correlations and experimental data for the two input methods considered. The correlations predict an inverse trend of the volume fraction as U_G increases with respect to the experimental data. However, the values obtained only deviate slightly from the experimental data. At the walls, a no-slip boundary condition is applied for the continuous phase and a free-slip condition is assigned for the disperse phase.

Proper setting of turbulent quantities at the inlet is still an open problem nowadays due to the complexity of two-phase phenomena and the lack of experimental data. We suggest to set turbulent quantities following the correlations of Kawase and Moo-Young (1989) for the bulk liquid turbulent kinematic viscosity, $\bar{\nu}_t$, and the average mixing length, $\bar{l}$, in bubble columns:

$$\bar{\nu}_t = \frac{1}{33.9} g^{1/3} d_c^{4/3} U_G^{1/3} \tag{17}$$

$$\bar{l} = 0.1 d_c \tag{18}$$

These give equations for the bulk liquid turbulent kinetic energy, $\bar{k}_L$, and bulk liquid turbulent dissipation rate, $\bar{\epsilon}_L$, in bubble columns:

$$\bar{k}_L = \left(\frac{\bar{\nu}_t}{\bar{l} C_\mu^{1/4}} \right)^2 \tag{19}$$

$$\bar{\epsilon}_L = C_\mu^{3/4} \frac{k^{3/2}}{\bar{l}} \tag{20}$$

Here, the factors $C_\mu^{1/4}$ and $C_\mu^{3/4}$ in the above equations ensure consistency with the definition of the turbulent length scales for two-equation turbulence models.

Table 5: Literature studies and code reference to Figure 3.

Code	Reference	d_c [m/s]	Aspect ratio [-]	Design
R1	Kawase and Moo-Young (1989)	0.24	22.1	Cylindrical
	correlation for our bubble column			
R2	Yao et al. (1991)	0.29	$5 \div 12$	Cylindrical
R3	Mudde et al. (1997)	$0.14 \div 0.23$	5	Cylindrical
R4	Sanyal et al. (1999)	0.19	2.8	Cylindrical
R5	Deen et al. (2001)	0.15	1.7	Squared
R6	Deen (2001)	0.15	5.2	Squared
R7	Vial et al. (2001)	0.10	10	Cylindrical
R8	Juliá et al. (2007)	0.264	$0.3 \div 2.25$	Rectangular
R9	Ojima et al. (2014)	0.20	3	Squared

The bulk liquid turbulent specific dissipation rate $\bar{\omega}_L$, is given as

$$\bar{\omega}_L = \frac{k^{1/2}}{\bar{l} C_\mu^{1/4}} \qquad (21)$$

and the average liquid velocity fluctuations, $\bar{u}'_L$ reads

$$\bar{u}'_L = \sqrt{\frac{2}{3} \bar{k}_L} \qquad (22)$$

These correlations are able to predict reasonably well experimental data of bulk liquid fluctuations from the literature. Figure 3 display the comparison between Eq. 22, in which $\bar{k}_L$ is estimated using the correlations of Kawase and Moo-Young (1989), and the experimental data listed in Table 5. A large scattering of the data is observed due to the various conditions considered and the uncertainties related to the measurements, however the main trend is captured by the correlation.

Eq. 19 and Eq. 21 are used to set the inlet and initial conditions of the liquid turbulent quantities. The lack of information on the gas phase drives us to set gas turbulent quantities as the liquid ones.
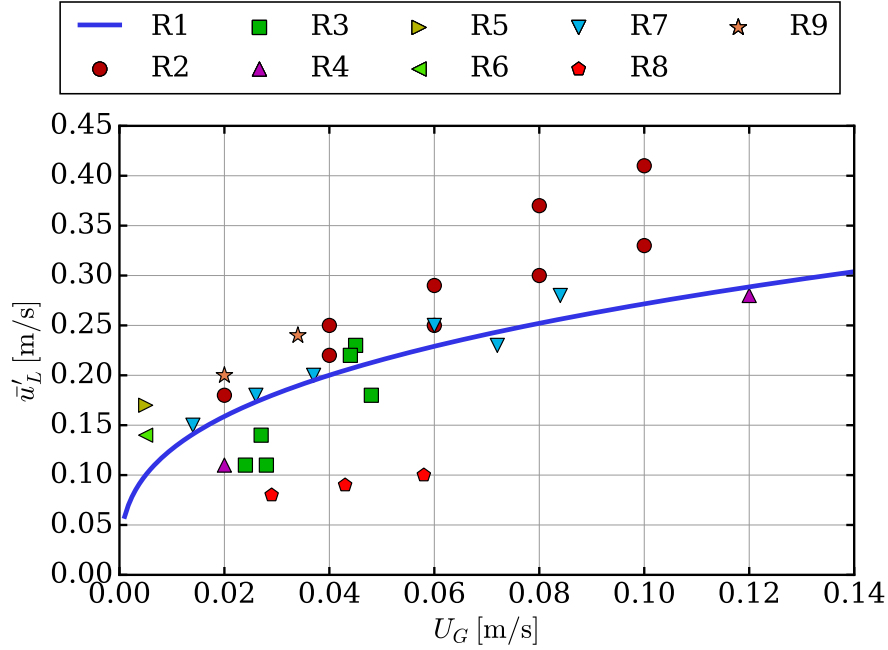
Figure 3: Comparison between Kawase and Moo-Young (1989) correlations and experimental data from the literature.

3.8. Numerical settings

Three-dimensional and transient simulations have been carried out. The various numerical schemes are chosen to reduce the discretization error as much as possible within the ANSYS Fluent CFD software. A second-order Euler implicit temporal discretization scheme is adopted. Gradients are estimated using a least squares cell-based method. The quadratic upstream interpolation for convective kinematics scheme is used to discretize the convection term of each scalar solved. A phase coupled semi-implicit method for pressure-linked equations (PC-SIMPLE) algorithm guarantees the coupling between pressure, velocity, and volume fraction. Under-relaxation factors are set respectively to 0.4 for the pressure and momentum equations and to 0.5 for the volume fraction, turbulent kinetic energy and turbulent specific dissipation rate equations. The time discretization is characterized by using the CFL number and, in this study,

$_{500}$ a CFL < 1 is considered. This criterion has shown to provide stable and rapidly $_{501}$ converging solutions of the system of equations at each time step. A time step $_{502}$ size sensitivity study has been carried out and the optimal value $\Delta t = 10^{-3}$ s $_{503}$ has been found, together with an optimal number of outer iterations per time $_{504}$ step of 20, ensuring maximum residual values below 3×10^{-5} for all the cases $_{505}$ investigated.

$_{506}$ 3.9. Numerical procedure

$_{507}$ The simulation procedure is similar to the one typically employed in transient $_{508}$ bubble column flow studies (Ziegenhein et al., 2015; Masood and Delgado, 2014; $_{509}$ Masood et al., 2014, 2015). The sequence followed in the simulations includes $_{510}$ an initial run to reach a statistical steady temporal convergence of the solution. $_{511}$ The first run has a duration of 50 s in physical time, and a second run of 30 $_{512}$ s is performed with data sampling to collect temporal averages and standard $_{513}$ deviations of the resolved variables. The duration of the first run is dictated by $_{514}$ the temporal evolution of the bulk holdup, i.e., the volume fraction calculated $_{515}$ within a volume for which $0.8 \leq h \leq 3.245$ m. When this quantity stabilizes, $_{516}$ it means that the flow is developed and that data sampling operations can be $_{517}$ performed.

$_{518}$ 4. Sensitivity study

$_{519}$ Sensitivity analyses on the mesh element size, time step size, and number of $_{520}$ outer iterations per time step were performed. For references, maximum relative $_{521}$ variations in the gas holdup of about 4% were obtained in the time step size $_{522}$ and number of outer iterations studies, when the *medium*, *fine*, and *optimized* $_{523}$ meshes were used (see Table 1 for the characteristics of the meshes). The largest $_{524}$ relative variations are obtained when the mesh element size is reduced. Thus, $_{525}$ for the sake of conciseness, only the study on the mesh element size is reported $_{526}$ in this paper.

$_{527}$ All the simulations are performed using the *arbitrary* input method and the $_{528}$ other settings listed in Section 3. Steady-state and statistically periodic tran-

23

Table 6: Mesh element size sensitivity study for $U_G = 0.0087$ m/s and $U_G = 0.0220$ m/s.

U_G	Mesh	$\epsilon_{G,\text{small}}$	$\epsilon_{G,\text{large}}$	$\epsilon_{G,\text{CFD}}$	$\epsilon_{G,\text{EXP}}$	Rel. Error [%]	Type
0.0087	*coarse*	0.0179	0.0034	0.0213	0.0287	-25.91	SS
	medium	0.0179	0.0037	0.0216	0.0287	-24.86	SS
	fine	0.0191	0.0053	0.0244	0.0287	-15.12	TR
	optimized	0.0189	0.0050	0.0239	0.0287	-16.86	TR
0.0220	*coarse*	0.0560	0.0060	0.0620	0.0750	-17.39	SS
	medium	0.0570	0.0132	0.0702	0.0750	-6.46	TR
	fine	0.0524	0.0188	0.0712	0.0750	-5.13	TR
	optimized	0.0547	0.0165	0.0712	0.0750	-5.13	TR

sient solutions are noticed, depending on the inlet air flow rate and mesh element size. In the following, these types of solution will be denoted, respectively, as SS and TR. Table 6 lists the results for two gas superficial velocities and the four investigated meshes. We note that a sufficiently fine mesh is required to capture the main transient phenomena of the problem, as the *coarse* and eventually the *medium* meshes lead to steady-state solutions. If the mesh resolution is too low, the accuracy of gradients estimates required in the computation of bubble forces, for instance, is compromised and flow instabilities are not resolved. The absence of flow instabilities in the solution leads to a significant reduction of the *large* bubbles holdup, which means that less dispersion of the *large* bubbles is obtained with coarse meshes. Table 7 lists additional results for diverse gas superficial velocities simulated with the *coarse* and *optimized* meshes. We note that even at higher flow rates, where instabilities are more readily to occur, simulations with the *coarse* mesh still exhibit steady-state solutions leading to high relative errors in the gas holdups when compared to experimental data.

Overall, the *optimized* mesh provides the best accuracy/performance ratio and is chosen for the remaining simulations. The particularity of this mesh lies in the increased transversal (horizontal) mesh element size with respect to the axial (vertical) one. This suggests that the solution is more sensitive to the

24

Table 7: Mesh element size sensitivity study for diverse U_G and the *coarse* and *optimized* meshes.

U_G	Mesh	$\epsilon_{G,\text{small}}$	$\epsilon_{G,\text{large}}$	$\epsilon_{G,\text{CFD}}$	$\epsilon_{G,\text{EXP}}$	Rel. Error [%]	Type
0.0043	*coarse*	0.0074	0.0023	0.0097	0.0143	-32.13	SS
	optimized	0.0079	0.0029	0.0108	0.0143	-24.43	TR
0.0065	*coarse*	0.0123	0.0029	0.0152	0.0217	-29.93	SS
	optimized	0.0132	0.0038	0.0170	0.0217	-21.64	TR
0.0087	*coarse*	0.0179	0.0034	0.0213	0.0287	-25.91	SS
	optimized	0.0189	0.0050	0.0239	0.0287	-16.86	TR
0.0109	*coarse*	0.0240	0.0038	0.0278	0.0361	-23.03	SS
	optimized	0.0248	0.0060	0.0308	0.0361	-14.73	TR
0.0131	*coarse*	0.0303	0.0042	0.0345	0.0435	-20.74	SS
	optimized	0.0308	0.0082	0.0390	0.0435	-10.41	TR
0.0153	*coarse*	0.0367	0.0046	0.0413	0.0509	-18.83	SS
	optimized	0.0369	0.0096	0.0465	0.0509	-8.61	TR
0.0175	*coarse*	0.0432	0.0051	0.0483	0.0590	-18.11	SS
	optimized	0.0428	0.0123	0.0551	0.0590	-6.58	TR
0.0198	*coarse*	0.0497	0.0055	0.0552	0.0686	-19.50	SS
	optimized	0.0489	0.0140	0.0629	0.0686	-8.27	TR
0.0220	*coarse*	0.0560	0.0060	0.0620	0.0750	-17.39	SS
	optimized	0.0547	0.0165	0.0712	0.0750	-5.13	TR
0.0243	*coarse*	0.0623	0.0064	0.0687	0.0830	-17.25	SS
	optimized	0.0601	0.0191	0.0792	0.0830	-4.61	TR
0.0266	*coarse*	0.0698	0.0070	0.0768	0.0888	-13.48	SS
	optimized	0.0662	0.0210	0.0872	0.0888	-1.77	TR

548 discretization in the directions transversal to the main flow, where gradients are
549 higher. Such conclusion is in accordance with the study by Ziegenhein et al.
550 (2015).

5. Results

552 Simulations of the air–water flow in the annular gap bubble column were
553 performed at gas superficial velocities ranging from 0.004 m/s to 0.225 m/s.
554 First a comparison between mono- and bi-dispersed approaches is presented,
555 highlighting the importance of considering separately small and large bubbles
556 dynamics. Then a comparison between input methodologies for the inlet gas
557 volume fraction and equivalent diameter of bubbles groups is carried out to
558 estimate the sensitivity of the predictions to the gas inlet data.

5.1. Comparison between mono- and bi-dispersed approaches

560 The proposed bi-dispersed Eulerian model is compared with two mono-
561 dispersed approaches corresponding to *(a)* small bubbles only and *(b)* large
562 bubbles only. The equivalent bubble diameters and inlet volume fractions for
563 the bi-dispersed model are set according to the *arbitrary* input mode. For the
564 mono-dispersed models, the inlet volume fractions of the bubbles groups are set
565 such that only small or large bubbles are present, and the equivalent bubble
566 diameters are set according to the *arbitrary* method.

567 Comparison of the holdup curves obtained using these models against ex-
568 perimental data is given in Figure 4. We note significant deviations from the
569 experimental data when the mono-dispersed approach is implemented. In par-
570 ticular, simulations with only small bubbles overestimate the gas holdup while
571 it is underestimated by simulations with only large bubbles. Qualitatively, we
572 observe that in the former cases, the initial non-uniformity due to the local gas
573 injection rapidly vanishes and the gas phase spreads all-over the column cross-
574 section, as depicted in Figure 5 for $U_G = 0.0220$ m/s. This phenomenon is due
575 to the positive lift coefficient that, in bubble columns, forces the small bubbles

26

to migrate from high volume fraction areas toward low volume fraction ones, resulting in a uniform spreading over the entire cross-section (the stabilizing effect of the lift force explained in Lucas et al. (2006)). The even distribution of small bubbles over the whole cross-section also reduces liquid recirculation and the gas holdup increases due to higher resistance. On the other hand, we observed that in the case of large bubbles only, the initial non-uniform gas distribution remains concentrated around the internal pipes long after the inlet section, as depicted in Figure 5, meaning that the spreading of the gas phase is much slower than for small bubbles. This leads to higher gas velocities and, as a result, to underestimated gas holdups. This is explained by the negative lift coefficient of large bubbles that forces them to migrate toward higher liquid velocity areas. In addition, a local increase of the gas volume fraction leads to a local increase of the liquid velocity, as a consequence large bubbles tend to move toward regions of higher gas volume fraction and local volume fraction disturbances are amplified. In this case, the lift force has therefore a destabilizing effect, as explained in Lucas et al. (2006). The only force that can counter-act this effect and disperse the bubbles is the turbulent dispersion force. In our simulations, the injection is local to one of the inner pipes and acts as a local disturbance in the gas volume fraction distribution. It is therefore reasonable to expect the bubbles plume to remain close to the inner pipes and only disperse slightly within the cross-section due to the effect of the turbulent dispersion force.

When both small and large bubbles groups are implemented, the gas holdups are much closer to the experimental ones for gas superficial velocities up to about 0.03 m/s. Qualitatively, we observe that the large bubbles concentrate principally near the internal pipes, as expected, while the small bubbles spread over the cross-section and are also accelerated by large bubbles, leading to local decreases in volume fraction, as illustrated in Figure 5 for the condition $U_G = 0.0220$ m/s. The combination of the stabilization, destabilization, and entrainment effects leads to intermediate overall gas holdups with respect to only small or large bubbles. These holdups values are more representative of

27
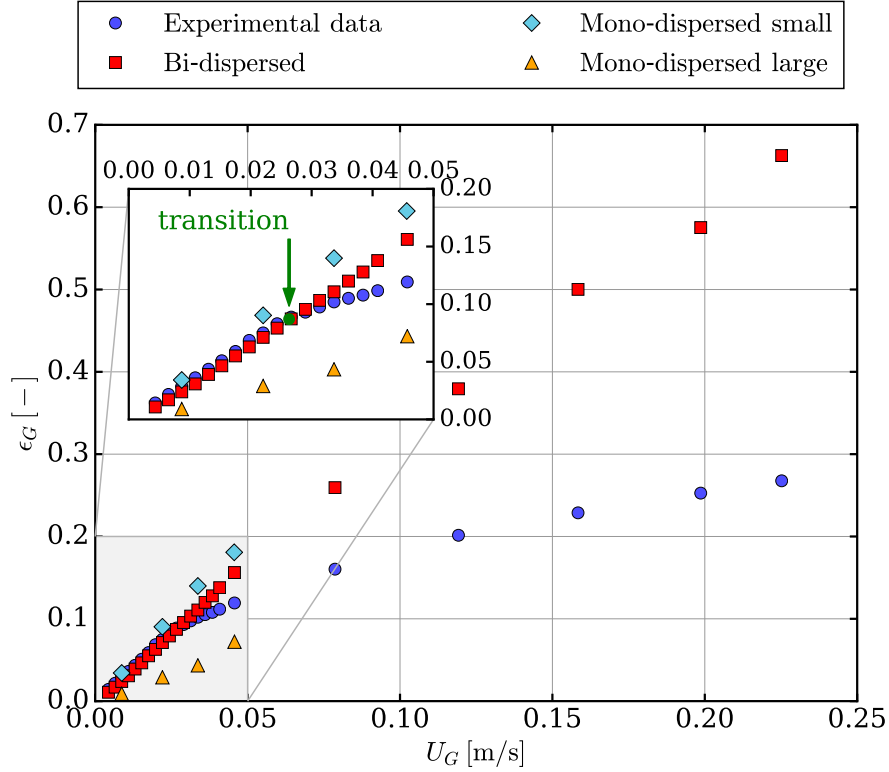
Figure 4: Comparison of holdup curves for mono- and bi-dispersed models against experimental data.

the experimental ones, suggesting that the modeled dynamics is closer to reality, at least up to $U_G \approx 0.03$ m/s. During the experiments, a gas transition superficial velocity of 0.0263 m/s was observed (Besagni and Inzoli, 2016a), suggesting that the proposed bi-dispersed model, with constant equivalent diameters, is not able to capture the dynamics occurring in the heterogeneous regime. In particular, as the gas flow rate increases, the collisions between bubbles intensify, resulting in a higher bubble coalescence rate. At some point, the coalescence rate reaches a critical value (the regime transition) and a significant amount of large bubbles forms from small bubbles within the whole cross-section, leading to the complete destabilization of the flow. Since the coalescence mechanism is not included in the present model, the destabilization of the flow remains lo-

28
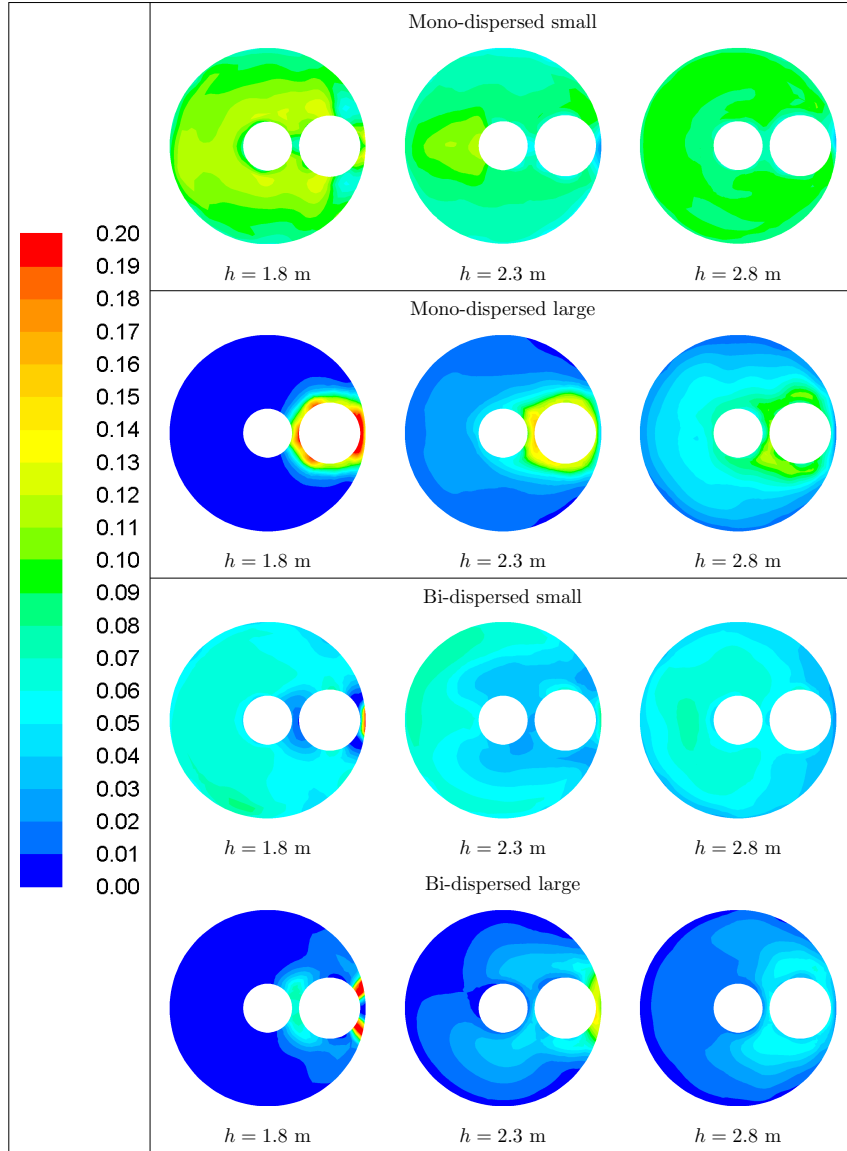
Figure 5: Comparison of volume fraction distributions on three horizontal cross-sections at $h = 1.8, 2.3$, and 2.8 m from the bottom of the column for $U_G = 0.0220$ m/s.

cal to the internal pipes, i.e., where large bubbles are initially released, and the small bubbles keep stabilizing the flow in the remaining part of the cross-section,

increasing the overall gas holdup.

We conclude that a bubble coalescence and breakup model may be fundamental for the correct description of the fluid dynamics in the heterogeneous regime, while a bi-dispersed approach is necessary to reliably predict the homogeneous flow regime in bubble column reactors. It is however worth noting that a mono-dispersed approach could be sufficient to simulate a so-called pure homogeneous regime, as the one observed in Mudde et al. (2009), i.e., a regime where bubble size distributions do not show large bubbles.

5.2. Comparison between input methods

A second analysis is performed and concerns the comparison between input methodologies for the equivalent bubble diameter and inlet volume fraction of the gas phases. The absence of experimental data often forces engineers to adopt values taken from other studies or from empirical correlations. However, the bubble size distributions in bubble column reactors are mainly dictated by the gas sparger type and configuration, diameter of the column and properties of the gas and liquid phases. Thus, data obtained from the cited methods can lead to significantly different equivalent diameters due to the variety of possible conditions. Here, experimental bubble size distributions for three gas superficial velocities are available (Besagni and Inzoli, 2016a). A comparison with the *arbitrary* input method is therefore proposed to evaluate the accuracy and sensitivity of the results to the input method.

Table 8 lists the data obtained from the respective simulations using the two different input methods. Both the methods are found to predict relatively well the experimental gas holdups. The variations in the predictions between the two modalities are most probably attributed to the different inlet volume fractions of the *small* and *large* bubbles groups, since the equivalent bubble diameters are very close in each case (a maximum relative variation of 2.5% in the bubble diameters is noticed between the input methods). In particular, the holdup of the *small* bubbles group is quite sensitive to the inlet volume fraction, as relative variations of up to 24% are observed in the holdup for variations in

30

Table 8: Results of simulations using the *arbitrary* and *experimental BSD* input modes.

U_G	Input mode	$\epsilon_{G,\text{small}}$	$\epsilon_{G,\text{large}}$	$\epsilon_{G,\text{CFD}}$	$\epsilon_{G,\text{EXP}}$	Rel. Error [%]
0.0087	*arbitrary*	0.0189	0.0050	0.0239	0.0287	-16.86
	exp. BSD	0.0206	0.0045	0.2510	0.0287	-12.69
0.0220	*arbitrary*	0.0547	0.0165	0.0712	0.0750	-5.13
	exp.BSD	0.0502	0.0157	0.0659	0.0750	-12.19
0.0313	*arbitrary*	0.0780	0.0253	0.1033	0.0975	5.93
	exp. BSD	0.0627	0.0242	0.0869	0.0975	-10.89

the inlet volume fraction of about the same amount, while the relative differences in the *large* bubbles group holdup are contained to a maximum of 11%. This higher sensitivity of small bubbles holdup to the inlet volume fraction is explained by the stabilizing effect they have on the two-phase flow, which has more consequences on the total gas holdup. Gathering information on the relative amount of small bubbles is therefore important for the accuracy of the numerical predictions.

We conclude that apart from the necessity of reliable estimates of bubble equivalent diameters, the relative amount of small and large bubbles is another parameter that is relevant in simulations involving a bi-dispersed approach.

6. Conclusions

We presented and discussed holdup results of transient three-dimensional simulations of an annular gap bubble column reactor using a bi-dispersed Eulerian model. The setup of the numerical simulations was described and correlations based on literature data for determining the inlet turbulence properties in bubble column reactors were proposed. Diverse sensitivity studies were performed to evaluate the relative dependency of the results to the mesh element size, time step size, and number of outer iterations per time step. We found that the highest dependency of the results to these parameters lie in the mesh element size. In particular, a sufficiently fine mesh was required to reproduce correctly

the main transient phenomena in the bubble column. A higher sensitivity of the results on the mesh element size in the transversal direction with respect to the axial direction was also demonstrated, suggesting that elongated elements in the axial direction can be used to optimize the computations. Consecutively, the bi-dispersed model was compared with two mono-dispersed models corresponding respectively to only small bubbles and only large bubbles. From the phenomenological point of view, it is widely recognized that small bubbles tends to stabilize the flow while large bubbles have a destabilizing effect. We found that a bi-dispersed approach was crucial for the accurate prediction of the holdup curve in the homogeneous regime, suggesting that larges bubbles, if present, should be resolved separately from small bubbles in order to capture the destabilizing and entrainment effects they produce on the flow. However, we note that a mono-dispersed approach could be sufficient to simulate a so-called pure homogeneous regime, i.e., a regime where large bubbles are absent. Comparing two approaches for the characterization of bubbles groups in terms of equivalent diameter and inlet volume fraction, we also found that the total gas holdup is sensitive to the small bubbles inlet volume fraction. Despite such sensitivity, the obtained results were satisfactory for both methods indicating that inlet volume fractions could be set from available empirical correlations or from experimental data. We note, though, that accurate estimates of such input data could be important in some cases. In the heterogeneous regime, where bubbles coalescence starts to play an important role in the two-phase flow dynamics, our proposed bi-dispersed model over-predicts the holdup curve due to obvious limitations. In particular, we expect the formation of large bubbles within the whole cross-section (due to coalescence) to destabilize significantly the fluids flow and as a result to decrease the gas holdup. The implementation of a population balance model able to describe bubbles coalescence and breakup phenomena is therefore presumed to improve significantly the accuracy of simulations in the heterogeneous regime, which is the prevailed regime in industrial applications, and is object of future developments.

Nomenclature

BSD	bubble size distribution
C_D	drag coefficient
C_L	lift coefficient
C_μ	model constant
C_{TD}	turbulent dispersion coefficient
C_{WL}	wall lubrication coefficient
CFD	computational fluids dynamics
CFL	Courant Friedrichs Lewy number
d_b	equivalent bubble diameter [m]
d_c	column inner diameter [m]
d_{holes}	distributor holes diameter [m]
$d_\perp$	maximum bubble horizontal dimension [m]
Eo	Eötvös number
$\mathbf{F}_D$	drag force [kg m^{-2} s^{-2}]
$\mathbf{F}_L$	lift force [kg m^{-2} s^{-2}]
$\mathbf{F}_{\text{TD}}$	turbulent dispersion force [kg m^{-2} s^{-2}]
$\mathbf{F}_{\text{VM}}$	virtual mass force [kg m^{-2} s^{-2}]
$\mathbf{F}_{\text{WL}}$	wall lubrication force [kg m^{-2} s^{-2}]
$\mathbf{g}$	gravity acceleration [m s^{-2}]
h	vertical position [m]
H_0	initial water free surface location [m]
H_c	column height [m]
k	turbulent kinetic energy [m^2 s^{-2}]
l	mixing length [m]
LES	large eddy simulation

$\mathbf{M_I}$ interfacial momentum exchanges term [kg m^{-2} s^{-2}]

n number of bubbles in a class

$\mathbf{n}_w$ unit normal to the wall pointing toward the fluid

p pressure [Pa]

PC-SIMPLE   phase coupled semi-implicit method for pressure-linked equations

RANS   Reynolds-averaged Navier-Stokes

Re_b bubble Reynolds number

RSM   Reynolds stress model

SST   shear-stress-transport

t time [s]

$\mathbf{u}$ velocity vector [m s^{-1}]

U_G gas superficial velocity [m s^{-1}]

U-RANS   unsteady Reynolds-averaged Navier-Stokes

y_w distance to the nearest wall

Greek letters

α volume fraction

Δt time step size [s]

ϵ turbulent dissipation rate [m^2 s^{-3}]

ϵ_G gas holdup

μ dynamic viscosity [kg m^{-1} s^{-1}]

ν kinematic viscosity [m^2 s^{-1}]

ω specific dissipation rate [s^{-1}]

ρ density [kg m^{-3}]

σ surface tension coefficient [N m^{-1}]

$\bar{\tau}$ viscous and Reynolds stresses tensor [kg m^{-1} s^{-2}]

Subscripts

G gas phase

j j-th dispersed phase

k k-th phase

large   large bubbles group

L liquid phase

small   small bubbles group

References

Al-Oufi, F.M., Cumming, I.W., Rielly, C.D., 2010. Destabilisation of homogeneous bubbly flow in an annular gap bubble column. The Canadian Journal of Chemical Engineering 88, 482–490. doi:10.1002/cjce.20301.

Al-Oufi, F.M., Rielly, C.D., Cumming, I.W., 2011. An experimental study of gas void fraction in dilute alcohol solutions in annular gas bubble columns using a four-point conductivity probe. Chemical Engineering Science 66, 5739–5748. doi:10.1016/j.ces.2011.03.061.

Antal, S.P., Lahey Jr, R.T., Flaherty, J.E., 1991. Analysis of phase distribution in fully developed laminar bubbly two-phase flow. International Journal of Multiphase Flow 17, 635–652. doi:10.1016/0301-9322(91)90029-3.

Becker, S., Sokolichin, A., Eigenberger, G., 1994. Gas–liquid flow in bubble columns and loop reactors: Part II. Comparison of detailed experiments and flow simulations. Chemical Engineering Science 49, 5747–5762. doi:10.1016/0009-2509(94)00290-8.

Behkish, A., Lemoine, R., Oukaci, R., Morsi, B.I., 2006. Novel correlations for gas holdup in large-scale slurry bubble column reactors operating under elevated pressures and temperatures. Chemical Engineering Journal 115, 157–171. doi:10.1016/j.cej.2005.10.006.

Besagni, G., Guédon, G.R., Inzoli, F., 2014a. Experimental and numerical study of counter-current flow in a vertical pipe, in: ASME 2014 12th Biennial Conference on Engineering Systems Design and Analysis, p. V002T11A009. doi:10.1115/ESDA2014-20122. iSBN: 978-0-7918-4584-4.

Besagni, G., Guédon, G.R., Inzoli, F., 2014b. Experimental investigation of counter current air-water flow in a large diameter vertical pipe with inners. Journal of Physics: Conference Series 547, 012024. doi:10.1088/1742-6596/547/1/012024.

Besagni, G., Guédon, G.R., Inzoli, F., 2016. Annular gap bubble column: Experimental investigation and computational fluid dynamics modeling. Journal of Fluids Engineering, Transactions of the ASME 138, 011302. doi:10.1115/1.4031002.

Besagni, G., Inzoli, F., 2016a. Bubble size distributions and shapes in annular gap bubble column. Experimental Thermal and Fluid Science 74, 27–48. doi:10.1016/j.expthermflusci.2015.11.020.

Besagni, G., Inzoli, F., 2016b. Comprehensive experimental investigation of counter-current bubble column hydrodynamics: Holdup, flow regime transition, bubble size distributions and local flow properties. Chemical Engineering Science 146, 256–290. doi:10.1016/j.ces.2016.02.043.

Besagni, G., Inzoli, F., 2016c. Influence of internals on counter-current bubble column hydrodynamics: Holdup, flow regime transition and local flow properties. Chemical Engineering Science 145, 162–180. doi:10.1016/j.ces.2016.02.019.

Borchers, O., Busch, C., Sokolichin, A., Eigenberger, G., 1999. Applicability of the standard k–ϵ turbulence model to the dynamic simulation of bubble columns. Part II: Comparison of detailed experiments and flow simulations. Chemical Engineering Science 54, 5927–5935. doi:10.1016/S0009-2509(99)00181-5.

Burns, A.D., Frank, T., Hamill, I., Shi, J.M., 2004. The Favre averaged drag model for turbulent dispersion in Eulerian multi-phase flows, in: 5th International Conference on Multiphase Flow, ICMF'04, Yokohama, Japan, May 30–June 4, 2004, Paper No. 392, pp. 1–17.

Buwa, V.V., Ranade, V.V., 2002. Dynamics of gas–liquid flow in a rectangular bubble column: experiments and single/multi-group CFD simulations. Chemical Engineering Science 57, 4715–4736. doi:10.1016/S0009-2509(02)00274-9.

36

Chen, P., Duduković, M.P., Sanyal, J., 2005a. Three-dimensional simulation of bubble column flows with bubble coalescence and breakup. A.I.Ch.E. Journal 51, 696–712. doi:10.1002/aic.10381.

Chen, P., Sanyal, J., Dudukovic, M.P., 2004. CFD modeling of bubble columns flows: implementation of population balance. Chemical Engineering Science 59, 5201–5207. doi:10.1016/j.ces.2004.07.037.

Chen, P., Sanyal, J., Duduković, M.P., 2005b. Numerical simulation of bubble columns flows: effect of different breakup and coalescence closures. Chemical Engineering Science 60, 1085–1101. doi:10.1016/j.ces.2004.09.070.

Cheung, S.C.P., Yeoh, G.H., Tu, J.Y., 2007a. On the modelling of population balance in isothermal vertical bubbly flows—Average bubble number density approach. Chemical Engineering and Processing: Process Intensification 46, 742–756. doi:10.1016/j.cep.2006.10.004.

Cheung, S.C.P., Yeoh, G.H., Tu, J.Y., 2007b. On the numerical study of isothermal vertical bubbly flow using two population balance approaches. Chemical Engineering Science 62, 4659–4674. doi:10.1016/j.ces.2007.05.030.

Colombo, M., Fairweather, M., 2015. Multiphase turbulence in bubbly flows: RANS simulations. International Journal of Multiphase Flow 77, 222–243. doi:10.1016/j.ijmultiphaseflow.2015.09.003.

Cumming, I.W., Rielly, C.D., Mason, A.J., 2002. Hydraulic performance of an annular plunging jet reactor. Chemical Engineering Research and Design 80, 543–549. doi:10.1205/026387602320224111.

Das, G., Das, P.K., Purohit, N.K., Mitra, A.K., 1999a. Flow pattern transition during gas liquid upflow through vertical concentric annuli—Part I: Experimental investigations. Journal of Fluids Engineering 121, 895–901. doi:10.1115/1.2823552.

Das, G., Das, P.K., Purohit, N.K., Mitra, A.K., 1999b. Flow pattern transition during gas liquid upflow through vertical concentric annuli—Part II: Mecha-

nistic models. Journal of Fluids Engineering 121, 902–907. doi:10.1115/1.2823553.

Deen, N., 2001. An Experimental and Computational Study of Fluid Dynamics in Gas-Liquid Chemical Reactors. Ph.D. thesis. Aalborg University.

Deen, N.G., Solberg, T., Hjertager, B.H., 2001. Large eddy simulation of the Gas–Liquid flow in a square cross-sectioned bubble column. Chemical Engineering Science 56, 6341–6349. doi:10.1016/S0009-2509(01)00249-4.

Dhotre, M.T., Niceno, B., Smith, B.L., 2008. Large eddy simulation of a bubble column using dynamic sub-grid scale model. Chemical Engineering Journal 136, 337–348. doi:10.1016/j.cej.2007.04.016.

Díaz, M.E., Iranzo, A., Cuadra, D., Barbero, R., Montes, F.J., Galán, M.A., 2008. Numerical simulation of the gas–liquid flow in a laboratory scale bubble column: Influence of bubble size distribution and non-drag forces. Chemical Engineering Journal 139, 363–379. doi:10.1016/j.cej.2007.08.015.

Díaz, M.E., Montes, F.J., Galán, M.A., 2009. Influence of the lift force closures on the numerical simulation of bubble plumes in a rectangular bubble column. Chemical Engineering Journal 64, 930–944. doi:10.1016/j.ces.2008.10.055.

Duan, X.Y., Cheung, S.C.P., Yeoh, G.H., Tu, J.Y., Krepper, E., Lucas, D., 2011. Gas–liquid flows in medium and large vertical pipes. Chemical Engineering Science 66, 872–883. doi:10.1016/j.ces.2010.11.031.

Dudukovic, M.P., 1999. Trends in catalytic reaction engineering. Catalysis Today 48, 5–15. doi:10.1016/S0920-5861(98)00353-8.

E. M. Cachaza, M.E.D., Montes, F.J., Galán, M.A., 2009. Simultaneous computational fluid dynamics (CFD) simulation of the hydrodynamics and mass transfer in a partially aerated bubble column. Industrial & Engineering Chemistry Research 48, 8685–8696. doi:10.1021/ie900314s.

Ekambara, K., Dhotre, M.T., 2010. CFD simulation of bubble column. Nuclear Engineering and Design 240, 963–969. doi:10.1016/j.nucengdes.2010.01.016.

Ekambara, K., Dhotre, M.T., Joshi, J.B., 2005. CFD simulations of bubble column reactors: 1D, 2D and 3D approach. Chemical Engineering Science 60, 6733–6746. doi:10.1016/j.ces.2005.05.047.

Frank, T., Zwart, P.J., Krepper, E., Prasser, H.M., Lucas, D., 2008. Validation of CFD models for mono- and polydisperse air–water two-phase flows in pipes. Nuclear Engineering and Design 238, 647–659. doi:10.1016/j.nucengdes.2007.02.056.

Grevskott, S., Sannaes, B.H., Duduković, M.P., Hjarbo, K.W., Svendsen, H.F., 1996. Liquid circulation, bubble size distributions, and solids movement in two- and three-phase bubble columns. Chemical Engineering Science 51, 1703–1713. doi:10.1016/0009-2509(96)00029-2.

Guillen, D.P., Grimmett, T., Gandrik, A.M., Antal, S.P., 2011. Development of a computational multiphase flow model for Fischer Tropsch synthesis in a slurry bubble column reactor. Chemical Engineering Journal 176–177, 83–94. doi:10.1016/j.cej.2011.08.078.

Hasan, A.R., Kabir, C.S., 1992. Two-phase flow in vertical and inclined annuli. International Journal of Multiphase Flow 18, 279–293. doi:10.1016/0301-9322(92)90089-Y.

Hosokawa, S., Tomiyama, A., Misaki, S., Hamada, T., 2002. Lateral migration of single bubbles due to the presence of wall, in: ASME 2002 Joint U.S.-European Fluids Engineering Division Conference, Montreal, Quebec, Canada, July 14–18, 2002, Paper No. FEDSM2002-31148, pp. 855–860. doi:10.1115/FEDSM2002-31148.

Jakobsen, H.A., 2002. Numerical convection algorithms and their role in Eu-

841 lerian CFD reactor simulations. International Journal of Chemical Reactor
842 Engineering 1, 1–16. doi:10.2202/1542-6580.1006.

843 Jakobsen, H.A., Lindborg, H., Dorao, C.A., 2005. Modeling of bubble column
844 reactors: Progress and limitations. Industrial & Engineering Chemistry Re-
845 search 44, 5107–5151. doi:10.1021/ie049447x.

846 Jakobsen, H.A., Sannaes, B.H., Grevskott, S., Svendsen, H.F., 1997. Modeling
847 of vertical bubble-driven flows. Industrial & Engineering Chemistry Research
848 36, 4052–4074. doi:10.1021/ie970276o.

849 Juliá, J.E., Hernández, L., Chiva, S., Vela, A., 2007. Hydrodynamic character-
850 ization of a needle sparger rectangular bubble column: Heterogeneous flow,
851 static bubble plume and oscillating bubble plume. Chemical Engineering Sci-
852 ence 62, 6361–6377. doi:10.1016/j.ces.2007.07.055.

853 Kawase, Y., Moo-Young, M., 1989. Turbulence intensity in bubble columns.
854 The Chemical Engineering Journal 40, 55–58. doi:10.1016/0300-9467(89)
855 80044-9.

856 Kelessidis, V.C., Dukler, A.E., 1989. Modeling flow pattern transitions for
857 upward gas–liquid flow in vertical concentric and eccentric annuli. Interna-
858 tional Journal of Multiphase Flow 15, 173–191. doi:10.1016/0301-9322(89)
859 90069-4.

860 Krepper, E., Lucas, D., Frank, T., Prasser, H.M., Zwart, P.J., 2008. The inho-
861 mogeneous MUSIG model for the simulation of polydispersed flows. Nuclear
862 Engineering and Design 238, 1690–1702. doi:10.1016/j.nucengdes.2008.
863 01.004.

864 Krepper, E., Lucas, D., Prasser, H.M., 2005. On the modelling of bubbly flow in
865 vertical pipes. Nuclear Engineering and Design 235, 597–611. doi:10.1016/
866 j.nucengdes.2004.09.006.

867 Krepper, E., Vanga, B.N.R., Zaruba, A., Prasser, H.M., Lopez de Bertodano,
868 M.A., 2007. Experimental and numerical studies of void fraction distribution

869 in rectangular bubble columns. Nuclear Engineering and Design 237, 399–408.
870 doi:10.1016/j.nucengdes.2006.07.009.

871 Krishna, R., van Baten, J.M., 2001. Eulerian simulations of bubble columns
872 operating at elevated pressures in the churn turbulent flow regime. Chemical
873 Engineering Science 56, 6249–6258. doi:10.1016/S0009-2509(01)00274-3.

874 Krishna, R., van Baten, J.M., Urseanu, M.I., 2000. Three-phase Eulerian
875 simulations of bubble column reactors operating in the churn-turbulent
876 regime: a scale up strategy. Chemical Engineering Science 55, 3275–3286.
877 doi:10.1016/S0009-2509(99)00582-5.

878 Krishna, R., Wilkinson, P.M., van Dierendonck, L.L., 1991. A model for gas
879 holdup in bubble columns incorporating the influence of gas density on flow
880 regime transitions. Chemical Engineering Science 46, 2491–2496. doi:10.
881 1016/0009-2509(91)80042-W.

882 Laborde-Boutet, C., Larachi, F., Dromard, N., Delsart, O., Schweich, D., 2009.
883 CFD simulation of bubble column flows: Investigations on turbulence models
884 in RANS approach. Chemical Engineering Science 64, 4399–4413. doi:10.
885 1016/j.ces.2009.07.009.

886 Lage, A.C.V.M., Time, R.W., 2002. An experimental and theoretical in-
887 vestigation of upward two-phase flow in annuli. SPE Journal 7, 325–336.
888 doi:10.2118/79512-PA.

889 Lakehal, D., Smith, B.L., Milelli, M., 2002. Large-eddy simulation of bubbly tur-
890 bulent shear flows. Journal of Turbulence 3, 1–21. doi:10.1088/1468-5248/
891 3/1/025.

892 Larachi, F., Desvigne, D., Donnat, L., Schweich, D., 2006. Simulating the effects
893 of liquid circulation in bubble columns with internals. Chemical Engineering
894 Science 61, 4195–4206. doi:10.1016/j.ces.2006.01.053.

Lehr, F., Mewes, D., 2001. A transport equation for the interfacial area density applied to bubble columns. Chemical Engineering Science 56, 1159–1166. doi:10.1016/S0009-2509(00)00335-3.

Lemoine, R., Behkish, A., Sehabiague, L., Heintz, Y.J., Oukaci, R., Morsi, B.I., 2008. An algorithm for predicting the hydrodynamic and mass transfer parameters in bubble column and slurry bubble column reactors. Fuel Processing Technology 89, 322–343. doi:10.1016/j.fuproc.2007.11.016.

Liao, Y., Lucas, D., Krepper, E., 2014. Application of new closure models for bubble coalescence and breakup to steam–water vertical pipe flow. Nuclear Engineering and Design 279, 126–136. doi:10.1016/j.nucengdes.2014.02.015.

Liao, Y., Rzehak, R., Lucas, D., Krepper, E., 2015. Baseline closure model for dispersed bubbly flow. Chemical Engineering Science 122, 336–349. doi:10.1016/j.ces.2014.09.042.

Lo, S.M., 1996. Application of the MUSIG model to bubbly flows. Technical Report. AEA Technology AEAT-1096.

Lucas, D., Krepper, E., Prasser, H.M., 2007. Use of models for lift, wall and turbulent dispersion forces acting on bubbles for poly-disperse flows. Chemical Engineering Science 62, 4146–4157. doi:10.1016/j.ces.2007.04.035.

Lucas, D., Krepper, E., Prasser, H.M., Manera, A., 2006. Investigations on the stability of the flow characteristics in a bubble column. Chemical Engineering & Technology 29, 1066–1072. doi:10.1002/ceat.200600150.

Lucas, D., Prasser, H.M., Manera, A., 2005. Influence of the lift force on the stability of a bubble column. Chemical Engineering Science 60, 3609–3619. doi:10.1016/j.ces.2005.02.032.

Lucas, D., Tomiyama, A., 2011. On the role of the lateral lift force in poly-dispersed bubbly flows. International Journal of Multiphase Flow 37, 1178–1190. doi:10.1016/j.ijmultiphaseflow.2011.05.009.

Ma, T., Lucas, D., Ziegenhein, T., Fröhlich, J., Deen, N.G., 2015a. Scale-Adaptive Simulation of a square cross-sectional bubble column. Chemical Engineering Science 131, 101–108. doi:10.1016/j.ces.2015.03.047.

Ma, T., Ziegenhein, T., Lucas, D., Fröhlich, J., 2016. Large eddy simulations of the gas–liquid flow in a rectangular bubble column. Nuclear Engineering and Design 299, 146–153. doi:10.1016/j.nucengdes.2015.08.010.

Ma, T., Ziegenhein, T., Lucas, D., Krepper, E., Fröhlich, J., 2015b. Euler–Euler large eddy simulations for dispersed turbulent bubbly flows. International Journal of Heat and Fluid Flow 56, 51–59. doi:10.1016/j.ijheatfluidflow.2015.06.009.

Masood, R.M.A., Delgado, A., 2014. Numerical investigation of the interphase forces and turbulence closure in 3d square bubble columns. Chemical Engineering Science 108, 154–168. doi:10.1016/j.ces.2014.01.004.

Masood, R.M.A., Khalid, Y., Delgado, A., 2015. Scale adaptive simulation of bubble column flows. Chemical Engineering Journal 262, 1126–1136. doi:10.1016/j.cej.2014.10.076.

Masood, R.M.A., Rauh, C., Delgado, A., 2014. CFD simulation of bubble column flows: An explicit algebraic Reynolds stress model approach. International Journal of Multiphase Flow 66, 11–25. doi:10.1016/j.ijmultiphaseflow.2014.06.008.

Milelli, M., 2002. A numerical analysis of confined turbulent bubble plumes. Ph.D. thesis. Swiss Federal Institute of Technology, Zürich. Diss. ETH. No. 14799.

Mudde, R.F., Groen, J.S., Van Den Akker, H.E.A., 1997. Liquid velocity field in a bubble column: LDA experiments. Chemical Engineering Science 52, 4217–4224. doi:10.1016/S0009-2509(97)88935-X.

Mudde, R.F., Harteveld, W.K., van den Akker, H.E.A., 2009. Uniform flow in bubble columns. Industrial & Engineering Chemistry Research 48, 148–158. doi:10.1021/ie8000748.

Mudde, R.F., Simonin, O., 1999. Two- and three-dimensional simulations of a bubble plume using a two-fluid model. Chemical Engineering Science 54, 5061–5069. doi:10.1016/S0009-2509(99)00234-1.

Nedeltchev, S., Shaikh, A., 2013. A new method for identification of the main transition velocities in multiphase reactors based on information entropy theory. Chemical Engineering Science 100, 2–14. doi:10.1016/j.ces.2013.03.039.

Oey, R.S., Mudde, R.F., van den Akker, H.E.A., 2003. Sensitivity study on interfacial closure laws in two-fluid bubbly flow simulations. A.I.Ch.E. Journal 49, 1621–1636. doi:10.1002/aic.690490703.

Ojima, S., Hayashi, K., Hosokawa, S., Tomiyama, A., 2014. Distributions of void fraction and liquid velocity in air–water bubble column. International Journal of Multiphase Flow 67, 111–121. doi:10.1016/j.ijmultiphaseflow.2014.05.008.

Pan, Y., Duduković, M.P., Chang, M., 1999. Dynamic simulation of bubbly flow in bubble columns. Chemical Engineering Science 54, 2481–2489. doi:10.1016/S0009-2509(98)00453-9.

Pfleger, D., Becker, S., 2001. Modelling and simulation of the dynamic flow behaviour in a bubble column. Chemical Engineering Science 56, 1737–1747. doi:10.1016/S0009-2509(00)00403-6.

Pfleger, D., Gomes, S., Gilbert, N., Wagner, H.G., 1999. Hydrodynamic simulations of laboratory scale bubble columns fundamental studies of the Eulerian–Eulerian modelling approach. Chemical Engineering Science 54, 5091–5099. doi:10.1016/S0009-2509(99)00261-4.

44

Pourtousi, M., Ganesan, P., Sahu, J.N., 2015a. Effect of bubble diameter size on prediction of flow pattern in Euler–Euler simulation of homogeneous bubble column regime. Measurement 76, 255–270. doi:10.1016/j.measurement.2015.08.018.

Pourtousi, M., Sahu, J.N., Ganesan, P., 2014. Effect of interfacial forces and turbulence models on predicting flow pattern inside the bubble column. Chemical Engineering and Processing 75, 38–47. doi:10.1016/j.cep.2013.11.001.

Pourtousi, M., Sahu, J.N., Ganesan, P., Shamshirband, S., Redzwan, G., 2015b. A combination of computational fluid dynamics (CFD) and adaptive neuro-fuzzy system (ANFIS) for prediction of the bubble column hydrodynamics. Powder Technology 274, 466–481. doi:10.1016/j.powtec.2015.01.038.

Pourtousi, M., Zeinali, M., Ganesan, P., Sahu, J.N., 2015c. Prediction of multi-phase flow pattern inside a 3D bubble column reactor using a combination of CFD and ANFIS. RSC Advances 5, 85652–85672. doi:10.1039/C5RA11583C.

Reilly, I.G., Scott, D.S., Debruijn, T.J.W., Macintyre, D., 1994. The role of gas phase momentum in determining gas holdup and hydrodynamic flow regimes in bubble column operations. The Canadian Journal of Chemical Engineering 72, 3–12. doi:10.1002/cjce.5450720102.

Ruzicka, M.C., Zahradník, J., Drahoš, J., Thomas, N.H., 2001. Homogeneous–heterogeneous regime transition in bubble columns. Chemical Engineering Science 56, 4609–4626. doi:10.1016/S0009-2509(01)00116-6.

Rzehak, R., Krepper, E., 2013. Closure models for turbulent bubbly flows: A CFD study. Nuclear Engineering and Design 265, 701–711. doi:10.1016/j.nucengdes.2013.09.003.

Rzehak, R., Krepper, E., Liao, Y., Ziegenhein, T., Kriebitzsch, S., Lucas, D., 2015. Baseline model for the simulation of bubbly flows. Chemical Engineering & Technology 38, 1972–1978. doi:10.1002/ceat.201500118.

Rzehak, R., Krepper, E., Lifante, C., 2012. Comparative study of wall-force models for the simulation of bubbly flows. Nuclear Engineering and Design 253, 41–49. doi:10.1016/j.nucengdes.2012.07.009.

Rzehak, R., Kriebitzsch, S., 2015. Multiphase CFD-simulation of bubbly pipe flow: A code comparison. International Journal of Multiphase Flow 68, 135–152. doi:10.1016/j.ijmultiphaseflow.2014.09.005.

Sanyal, J., Vásquez, S., Roy, S., Dudukovic, M.P., 1999. Numerical simulation of gas–liquid dynamics in cylindrical bubble column reactors. Chemical Engineering Science 54, 5071–5083. doi:10.1016/S0009-2509(99)00235-3.

Shah, Y.T., Kelkar, B.G., Godbole, S.P., Deckwer, W.D., 1982. Design parameters estimations for bubble column reactors. A.I.Ch.E. Journal 28, 353–379. doi:10.1002/aic.690280302.

Sokolichin, A., Eigenberger, G., 1994. Gas–liquid flow in bubble columns and loop reactors: Part I. Detailed modelling and numerical simulation. Chemical Engineering Science 49, 5735–5746. doi:10.1016/0009-2509(94)00289-4.

Sokolichin, A., Eigenberger, G., 1999. Applicability of the standard k–ϵ turbulence model to the dynamic simulation of bubble columns. Part I: Detailed numerical simulations. Chemical Engineering Science 54, 2273–2284. doi:10.1016/S0009-2509(98)00420-5.

Sokolichin, A., Eigenberger, G., Lapin, A., Lübert, A., 1997. Dynamic numerical simulation of gas–liquid two-phase flows Euler/Euler versus Euler/Lagrange. Chemical Engineering Science 52, 611–626. doi:10.1016/S0009-2509(96)00425-3.

Tabib, M.V., Roy, S.A., Joshi, J.B., 2008. CFD simulation of bubble column— An analysis of interphase forces and turbulence models. Chemical Engineering Journal 139, 589–614. doi:10.1016/j.cej.2007.09.015.

Tarmy, B.L., Coulaloglou, C.A., 1992. Alpha - omega and beyond industrial view of gas/liquid/solid reactor development. Chemical Engineering Science 47, 3231–3246. doi:10.1016/0009-2509(92)85031-6.

Tomiyama, A., Kataoka, I., Zun, I., Sakaguchi, T., 1998. Drag coefficients of single bubbles under normal and micro gravity conditions. JSME International Journal. Ser. B, Fluids and Thermal Engineering 41, 472–479. URL: http://ci.nii.ac.jp/naid/110002981557/en/.

Tomiyama, A., Tamai, H., Zun, I., Hosokawa, S., 2002. Transverse migration of single bubbles in simple shear flows. Chemical Engineering Science 57, 1849–1858. doi:10.1016/S0009-2509(02)00085-4.

van Baten, J.M., Krishna, R., 2001. Eulerian simulations for determination of the axial dispersion of liquid and gas phases in bubble columns operating in the churn-turbulent regime. Chemical Engineering Science 56, 503–512. doi:10.1016/S0009-2509(00)00254-2.

van Baten, J.M., Krishna, R., 2002. CFD simulations of a bubble column operating in the homogeneous and heterogeneous flow regimes. Chemical Engineering & Technology 25, 1081–1086. doi:10.1002/1521-4125(20021105)25:11<1081::AID-CEAT1081>3.0.CO;2-Y.

Vial, C., Lainé, R., Poncin, S., Midoux, N., Wild, G., 2001. Influence of gas distribution and regime transitions on liquid velocity and turbulence in a 3-D bubble column. Chemical Engineering Science 56, 1085–1093. doi:10.1016/S0009-2509(00)00325-0.

Wellek, R.M., Agrawal, A.K., Skelland, A.H.P., 1966. Shape of liquid drops moving in liquid media. A.I.Ch.E. Journal 12, 854–862. doi:10.1002/aic.690120506.

Xu, L., Yuan, B., Ni, H., Chen, C., 2013. Numerical simulation of bubble column flows in churn-turbulent regime: comparison of bubble size models. Industrial & Engineering Chemistry Research 52, 6794–6802. doi:10.1021/ie4005964.

Yao, B.P., Zheng, C., Gasche, H.E., Hofmann, H., 1991. Bubble behaviour and flow structure of bubble columns. Chemical Engineering and Processing: Process Intensification 29, 65–75. doi:10.1016/0255-2701(91)87015-U.

Youssef, A.A., Al-Dahhan, M.H., Dudukovic, M.P., 2013. Bubble columns with internals: A review. International Journal of Chemical Reactor Engineering 11, 169–223. doi:10.1515/ijcre-2012-0023.

Zhang, D., Deen, N.G., Kuipers, J.A.M., 2006. Numerical simulation of the dynamic flow behavior in a bubble column: A study of closures for turbulence and interface forces. Chemical Engineering Science 61, 7593–7608. doi:10.1016/j.ces.2006.08.053.

Ziegenhein, T., Rzehak, R., Lucas, D., 2015. Transient simulation for large scale flow in bubble columns. Chemical Engineering Science 122, 1–13. doi:10.1016/j.ces.2014.09.022.